Assessing the Projected Changes in European Air Stagnation due to Climate Change

JACOB W. MADDISON,[a] MARTA ABALOS,[a] DAVID BARRIOPEDRO,[b] RICARDO GARCÍA-HERRERA,[a,b] JOSE M. GARRIDO-PEREZ,[a] CARLOS ORDÓÑEZ,[a] AND ISLA R. SIMPSON[c]

[a] *Department of Earth Physics and Astrophysics, Universidad Complutense de Madrid, Madrid, Spain*
[b] *Instituto de Geociencias, CSIC-UCM, Madrid, Spain*
[c] *Climate and Global Dynamics, National Center for Atmospheric Research, Boulder, Colorado*

(Manuscript received 16 March 2022, in final form 15 September 2022)

ABSTRACT: Air pollution is a major environmental threat to human health. Pollutants can reach extreme levels in the lower atmosphere when weather conditions permit. As pollutant concentrations depend on scales and processes that are not fully represented in current global circulation models (GCMs), and it is often too computationally expensive to run models with atmospheric chemistry and aerosol processes, air stagnation is often used as a proxy for pollution events with particular success in Europe. However, the variables required to identify air stagnation can have biases in GCM output, which adds uncertainty to projected trends in air stagnation. Here, the representation of air stagnation in GCMs is assessed for Europe in the historical period and in end-of-century projections based on a high-emission scenario using three methods for identifying air stagnation. The monthly frequency of stagnation during summer and autumn is projected to increase with climate change when stagnation is identified by a well-established index. However, this increase is not present when air-stagnation frequency is estimated using a statistical model based on the synoptic- to large-scale atmospheric circulation. This implies that the projected increases in air stagnation are not driven by an increase in frequency or severity of large-scale circulation events that are conducive to stagnation. Indeed, projected changes to the atmospheric circulation in GCMs, in particular a reduction in atmospheric block frequency, would suggest a reduction in future air stagnation. Additional analyses indicate that the projected increases in stagnation frequency follow the trend toward more frequent dry days, which is apparently unrelated to the large-scale drivers of air stagnation.

KEYWORDS: Atmospheric circulation; Regression analysis; Climate models; Air quality

1. Introduction

Air stagnation refers to a period when a stable air mass develops over a given region and becomes almost stationary. Within the stagnant air mass, winds are weak and there is no precipitation. Such conditions are favorable for the buildup of pollutants in the lowest levels of the atmosphere (e.g., Leibensperger et al. 2008; Jacob and Winner 2009; Barmpadimos et al. 2011; Dawson et al. 2014; Garrido-Perez et al. 2019, 2021), where they can reach levels that are harmful for humans (WHO 2021; European Environment Agency 2020). Understanding how these events occur and how their frequency may change as a result of climate change is therefore of great importance to society. As direct pollutant measurements often have limited temporal and spatial coverage, identifying air-stagnation events offers an alternative approach for estimating pollutant concentrations by capturing weather conditions that may support their accumulation.

The success of air stagnation as an indicator for the concentration of a particular pollutant depends on various factors such as the region of the globe being considered and the season, as well as the pollutant species (Oswald et al. 2015; Kerr and Waugh 2018; Huang et al. 2018; Gao et al. 2020). For example, extreme pollution events associated with the advection of pollutants (e.g., Carro-Calvo et al. 2017; Garrido-Perez et al. 2019) are hardly accounted for in stagnation indices since the relatively strong winds facilitating the advection would preclude their definition as stagnant. In spite of this, stagnation indices generally perform well for pollution in Europe where air stagnation is strongly correlated to, and associated with significant enhancements of, pollutant concentrations (Garrido-Perez et al. 2018, 2021). Air stagnation also becomes valuable when attempting to describe pollutant levels in global circulation models (GCMs). In GCM output, pollutant data can be severely limited because the models have a coarser resolution than the scales on which pollutant concentrations depend. In addition, including atmospheric chemistry and aerosol processes in GCMs increases the computing time considerably due to the complicated chemistry and microphysics governing their interactions.

Identifying air stagnation from GCM output is not straightforward, either, as it also depends on scales not resolved in GCMs. Stagnant conditions can arise due to different processes depending on the region being considered, because local wind speed and precipitation are related to local characteristics such as orography, surface roughness, and urbanization. Accordingly, many air-stagnation indices (ASIs) exist (e.g., Horton et al. 2012, 2014; Huang et al. 2018; Wang et al. 2018; Gao et al. 2020). In this article, we use the adaptation of the National Climate Data Center air-stagnation index (Wang and Angell 1999) introduced in Horton et al. (2012, 2014).

Supplemental information related to this paper is available at the Journals Online website: https://doi.org/10.1175/JCLI-D-22-0180.s1.

Corresponding author: Jacob W. Maddison, jacobmad@ucm.es

DOI: 10.1175/JCLI-D-22-0180.1

This identifies air stagnation when 10 m (or surface) wind speed, 500 hPa wind speed, and precipitation are concurrently below certain absolute thresholds. This index is related to pollution events in Europe (Garrido-Perez et al. 2018, 2021; Maddison et al. 2021) and allows for the interpretation of air stagnation in GCMs in terms of potential pollutant impacts. As the variables used in ASIs can have considerable biases in GCMs (Meehl et al. 2007; Christensen et al. 2008; Catto et al. 2013; Flato et al. 2013; Kumar et al. 2013; Mehran et al. 2014), projected future increases in air stagnation (Horton et al. 2012, 2014; Caserini et al. 2017; Gao et al. 2020; Lee et al. 2020) may be uncertain and warrant further investigation, particularly concerning the driving factors of such increases and their sensitivity to GCM biases.

Local surface conditions are often strongly governed by the larger-scale atmospheric circulation (from synoptic to planetary scales). As such, the occurrence of air stagnation has been related to synoptic-scale weather systems and large-scale features of the circulation including atmospheric blocking events (Hamburger et al. 2011; Garrido-Perez et al. 2017; Ordóñez et al. 2017; Vautard et al. 2018; Webber et al. 2017), extratropical cyclones (Leibensperger et al. 2008; Tai et al. 2010, 2012; Leung et al. 2018), and the midlatitude jet streams (Shen et al. 2015; Ordóñez et al. 2019). Based on this knowledge, Maddison et al. (2021) constructed a stepwise multilinear regression model of the monthly air-stagnation variability in various regions within Europe. Robust, statistically significant relationships were found between air stagnation and the model predictors (synoptic-scale weather systems and large-scale flow features), which were able to explain between 40% and 70% of the variability in air stagnation. Therefore, this statistical model provides an alternative approach to ASIs for describing air stagnation in GCMs. As this model only relies on the dynamical aspects that drive air stagnation, it also allows the role of the dynamics in the projected air-stagnation trends to be addressed.

In this article, we assess the representation of air stagnation in GCMs and its projected future changes over Europe. For this assessment, air stagnation is identified in GCMs in three different ways (section 2b) to address the influence of GCM biases and of the large-scale circulation on the projected changes. The following research questions are addressed: 1) How well do GCMs represent air stagnation and what do they predict for future trends? 2) What is the impact of different stagnation indices on the simulated air-stagnation trends? 3) To what extent are the projected trends in air stagnation associated with dynamical changes?

This article is organized as follows. In section 2, the data and methods used throughout are summarized. Climate model biases are presented in section 3 for the variables used in the analyses. Air stagnation in the historical period is assessed in GCMs in section 4. In section 5, future changes in air stagnation are explored and the mechanisms driving the trends are discussed. The article is concluded in section 6.

2. Data and methods

The GCM simulations are from phase six of the Coupled Model Intercomparison Project (CMIP6) of the World Climate Research Programme (Eyring et al. 2016) and are described in section 2a. Data from the European Centre for Medium-Range Weather Forecasts' global reanalysis (ERA5; Hersbach et al. 2020) are used to verify the climate model simulations during the historical period. The predecessor of ERA5, ERA-Interim, already reproduced the observed spatiotemporal patterns of stagnation over Europe (Garrido-Perez et al. 2018), and the features found in ERA5 resemble those of ERA-Interim (Garrido-Perez et al. 2021, 2022). Climate change projections are assessed for the shared socioeconomic pathway (SSP) with strongest radiative forcing at the end of the twenty-first century (SSP5–8.5), which would result from continued high emissions of greenhouse gases (O'Neill et al. 2016). Note that global emissions of near-term climate forcers (aerosols and chemically reactive gases) are lower in the SSP5–8.5 scenario than in SSP3–7.0 (Riahi et al. 2017). Further note that the SSP5–8.5 scenario is seen as worst case and is unlikely to happen in reality. It is used here to obtain clear signals in the climate change response and for direct comparison with other air-stagnation studies that also consider high-emission scenarios (e.g., Horton et al. 2014; Garrido-Perez et al. 2022).

a. CMIP6 model output

The 20 GCMs from the CMIP6 archive that are used in this study are listed in Table 1. Thirty-year periods from the historical simulations (1981–2010) and future climate scenario SSP5–8.5 (2071–2100) are analyzed to compare present and future climates. One member from the ensemble of simulations run at each modeling center is included in the analysis, and its variant label is listed in Table 1. There is great variety in the CMIP6 models' setup, including their spatial resolutions (both horizontal and vertical). For this analysis, all model data have been interpolated horizontally to a common grid (2.5° × 2.5°). The variables accessed include surface wind speed (sfcwind), wind speed at 500 hPa (ws_500), precipitation (prec), zonal wind at 850 (u_850) and 250 hPa (u_250), and geopotential height at 500 hPa (zg_500). Daily average values of the variables are used in each case.

Robust signals are identified by quantifying the agreement among the climate models in simulating an observed feature or forced response. Agreement is here defined as when more than two-thirds of the GCMs agree on the sign of the feature of interest.

b. Air stagnation identification

We use three approaches to identify air stagnation from GCM output. Two of them directly calculate air stagnation monthly frequencies using the Horton et al. (2012, 2014) ASI, and one estimates these frequencies from the synoptic- to large-scale dynamical drivers of air stagnation using the statistical model of Maddison et al. (2021) (described below).

1) Stagnation is identified with the Horton ASI by imposing the thresholds for precipitation, surface wind speed, and 500 hPa wind speed used and verified in previous studies (e.g., Garrido-Perez et al. 2018), namely, daily precipitation less than 1 mm (a dry day), daily mean surface wind speed less than 3.2 m s^{-1}, and daily mean 500 hPa wind

TABLE 1. Summary of the CMIP6 models used in this article. The model resolution in latitude and longitude is represented as the number of points along a meridian and around a longitude circle, respectively.

Institute ID	Model version	Atmospheric resolution (lat, lon, levels)	Variant label
CSIRO-ARCCSS, Victoria, Australia	ACCESS-CM2	145, 192, L85	r1i1p1f1
CCCma, Victoria, Canada	CanESM5	64, 128, L49	r1i1p2f1
NCAR, Boulder, United States	CESM2	192, 288, L32	r4i1p1f1
	CESM2-WACCM	192, 288, L70	r1i1p1f1
EC-Earth-Consortium, Europe	EC-Earth3	256, 152, L91	r1i1p1f1
CAS, Beijing, China	FGOALS-g3	80, 180, L26	r1i1p1f1
MOHC, Exeter, United Kingdom	HadGEM3-GC31-LL	144, 192, L85	r1i1p1f3
	HadGEM3-GC31-MM	324, 432, L85	r1i1p1f3
INM, Moscow, Russia	INM-CM4-8	120, 180, L21	r1i1p1f1
	INM-CM5-0	120, 180, L73	r1i1p1f1
IPSL, Paris, France	IPSL-CM6A-LR	143, 144, L79	r1i1p1f1
AORI/NIES/JAMSTEC, Japan	MIROC6	128, 256, L81	r1i1p1f1
	MIROC-ES2L	64, 128, L40	r1i1p1f2
MPIM, Hamburg, Germany	MPI-ESM1-2-HR	192, 384, L95	r1i1p1f1
	MPI-ESM1-2-LR	96, 192, L47	r1i1p1f1
MRI, Tsukuba, Japan	MRI-ESM2-0	160, 320, L80	r1i1p1f1
NCC, Norway	NorESM2-LM	96, 144, L32	r1i1p1f1
	NorEMS2-MM	192, 288, L32	r1i1p1f1
AS-RCEC, Taipei, Taiwan	TaiESM1	0.9, 1.25, L30	r1i1p1f1
MOHC-NERC, United Kingdom	UKESM1-0-LL	144, 192, L85	r1i1p1f2

speed less than 13 m s^{-1}. This method is named nonpercentile adjusted (NPA) in the remainder of this article and is also applied for stagnation identification in ERA5.

2) Stagnation is identified as in method 1 but with the thresholds on surface wind speed, 500 hPa wind speed, and precipitation changed in each GCM to account for model biases in the occurrence of conditions defining the ASI. Following Garrido-Perez et al. (2022), thresholds are redefined at each grid point so that the ASI component frequencies during the historical period are the same in the GCM simulations as in ERA5. This is achieved by calculating the local percentiles of surface and 500 hPa wind speed and precipitation in each GCM that correspond to the respective ERA5 percentiles of the thresholds used in method 1. Note that this approach does not alter the output variables from the GCMs directly as in standard bias-correction methods but the local thresholds required for the identification of air-stagnation events. The resulting ASI is named percentile adjusted (PA). The thresholds in the PA ASI are generally lower than in the NPA ASI for 500 hPa wind speed and higher for precipitation and surface wind speed. However, these changes are typically small and still represent reasonable threshold values for stagnant conditions [see supplementary Fig. 2 in Garrido-Perez et al. (2022)].
3) Stagnation is estimated by the statistical model. This method, named the large-scale prediction (LS), is based on that of Maddison et al. (2021), in which a stepwise multilinear regression was constructed with ERA5 to model the monthly frequency in the Horton ASI for each season and for five European regions. The predictors included in the model were the monthly frequencies of blocking, Rossby wave breaking, and subtropical ridge events, as well as the monthly mean jet latitudes and speeds for the eddy-driven and subtropical jets. The variables required to calculate these predictors are the zonal wind (eddy-driven and subtropical jets), geopotential height (blocking and subtropical ridges), and potential temperature on the dynamical tropopause (Rossby wave breaking). As the latter is not included in the output of the CMIP6 models, we first redesigned the ERA5 statistical model of Maddison et al. (2021) with the Rossby wave breaking predictor removed. The skill of the new statistical model was only slightly reduced and remained statistically significant (not shown) and thus continues to be useful for studying stagnation variability.

To identify the regional monthly stagnation frequencies in the LS ASI we calculate the GCM time series for blocking, ridges, and the two jet stream indices. Blocking is identified using the flow reversal index of Scherrer et al. (2006) based on 500 hPa geopotential height. Ridges are also identified in the 500 hPa geopotential height field as subtropical intrusions of anomalously high geopotential following the method of Sousa et al. (2018). The approach of Woollings et al. (2010) identifies the eddy-driven jet latitude and intensity from midtropospheric winds and is adapted to also identify the subtropical jet parameters from upper-tropospheric winds. Full details on each of the indices is given in Maddison et al. (2021). These GCM predictors are then input into the statistical model obtained from ERA5, i.e., we take the ERA5 model coefficients and intercept to calculate the monthly LS ASI frequency in each region, season, and GCM simulation. This way, we avoid computing the ASI frequency from the simulated concurrence of unusual conditions on local scales, for which GCMs can have large biases. The LS ASI only informs on stagnation changes driven by

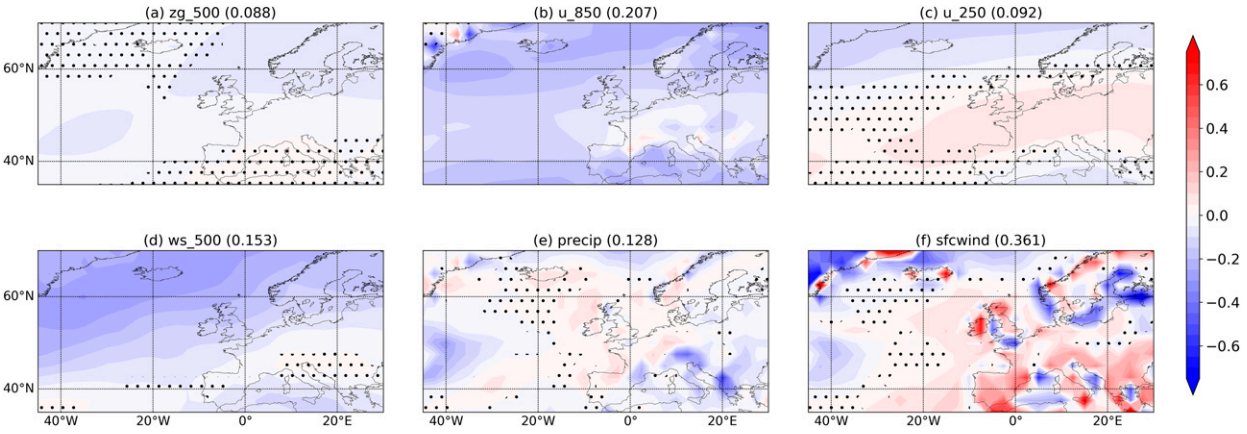

FIG. 1. Multimodel mean biases (normalized by the daily standard deviation of the reanalysis) in the annual historical (1981–2010) means of (a) geopotential height at 500 hPa (zg_500), (b) zonal wind at 850 hPa (u_850), (c) zonal wind at 250 hPa (u_250), (d) wind speed at 500 hPa (ws_500), (e) precipitation (precip), and (f) surface wind (sfcwind). Stippling shows where less than two-thirds of the GCMs agree on the sign of the bias. The numbers in parentheses show ensemble-mean RMSE values of the mean daily fields.

the large-scale atmospheric circulation, and hence it cannot provide a complete description of the true ASI variability (explained variances are between 40% and 70%).

The assumption that the ERA5 model can be used to identify air stagnation in GCMs will be tested in section 4. When assessing stagnation in the future, we also assume that its relationship with the synoptic- to large-scale circulation does not vary with time, and we test whether this is the case in section 5b. A further test is performed whereby the projected changes in the LS ASI are obtained from statistical models fully based on the GCM output (i.e., the simulated ASI and predictors of each GCM). We focus on the ERA5-based statistical model in the article but compare to GCM-based models where appropriate.

Throughout the article, each method will be tested in its ability to reproduce monthly frequencies of air stagnation in five distinct regions of Europe and for the four seasons. The five regions considered have been shown to exhibit distinct characteristics of stagnation (Garrido-Perez et al. 2018) and were also considered by Maddison et al. (2021) in the construction of the statistical model used in this article; they are Scandinavia (SCAN) and northern (NEU), central (CEU), southwestern (SW), and southeastern (SE) Europe (shown in Fig. 3a).

3. Model biases

CMIP6 model biases in the three ASIs' components are summarized in this section. Two types of bias (defined as model minus ERA5 differences) are considered for the assessed atmospheric fields: the bias in the mean and the bias in the daily standard deviation. They are not representative of all types of biases that may be important for air stagnation but provide a basic estimate of the GCMs' ability to reproduce these variables. Biases are calculated for each grid point and GCM separately and then normalized by the standard deviation of the corresponding variable in the reanalysis. Standardization is required for a fair comparison of the bias among variables with different magnitudes, variability, and units. In addition, we evaluate the spatial mean error over the considered domain for each GCM. To avoid spatial compensation of over- and underestimations, these overall errors are quantified as the root-mean-square error (RMSE). Finally, the multimodel mean of the aforementioned metrics is computed by averaging over the ensemble.

The multimodel mean biases of the variables used in the three stagnation indices for the historical period are shown in Fig. 1. They are generally higher for the variables used in ASIs (Figs. 1d–f), particularly over Europe, and lower for the predictors of the statistical model (Figs. 1a–c). Biases for zg_500 and u_250 are particularly low (Figs. 1a,c). GCMs tend to underestimate the wind speed in the lower to midtroposphere (Figs. 1b,d), though this is stronger over the Atlantic Ocean than the European continent. Lack of stippling indicates that this wind speed underestimation is common among the GCMs considered. Surface wind speed biases tend to be highest near coastlines and mountainous regions, pointing to land–sea and orographic effects (Fig. 1f). Moreover, there is a robust and substantial overestimation of surface wind over southern Europe. Precipitation is also underestimated across much of the region (particularly to the east; Fig. 1e), with generally smaller biases elsewhere.

The mean bias in the daily standard deviation of the same variables is shown in Fig. 2 (note that they are scaled by the standard deviation of the reanalysis field). These biases are generally consistent among the GCMs considered. Like the biases in the mean, the biases in the standard deviation of zg_500 and u_250 are low (Figs. 2a,c). The variability of the zonal wind in the lower troposphere is underestimated in the GCMs (Fig. 2b), the same as for the mean (Fig. 1b). The largest difference between the GCMs and ERA5 is seen for precipitation variability, which is substantially underestimated (especially around the Mediterranean). GCMs can struggle to represent extreme high-rainfall events, as shown in other studies (e.g., Sillmann et al. 2013; Mehran et al. 2014). GCMs have somewhat more variability than ERA5 in surface wind over Europe (Fig. 2f),

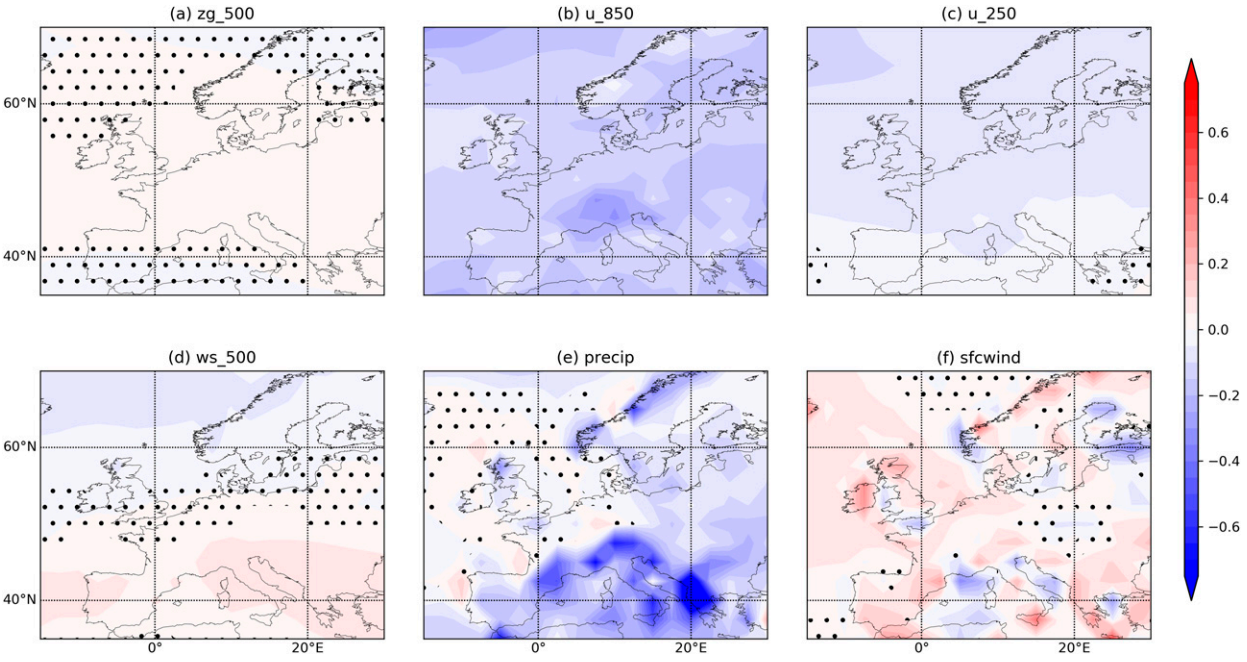

FIG. 2. Multimodel-mean biases (normalized by the daily standard deviation of the reanalysis) in the annual historical (1981–2010) variability (daily standard deviation) of the same fields in Fig. 1. Stippling shows where less than two-thirds of the GCMs agree on the sign of the bias.

particularly around coastlines, likely due to discrepancies and/or underrepresentation of subgrid processes.

In summary, the biases in the GCMs for the variables used in the ASI are generally higher than for the predictors of the statistical model for stagnation. Precipitation biases are particularly evident in the GCMs. However, it is worth noting that precipitation biases tend to be strongest for high-rainfall events (Mehran et al. 2014), which is also reflected in the reduced variability in the simulated precipitation shown here, and that GCMs may have smaller biases when simulating dry days (Sillmann et al. 2013), the latter being more important for air-stagnation events.

4. Air stagnation in the historical period

In this section, we assess the ability of the three methods described in section 2b to reproduce the historical monthly frequency of air stagnation. They are compared to the monthly frequency of the ASI in ERA5 during the same period. The ERA5 monthly frequency of stagnation is shown for each region (SCAN, NEU, CEU, SW, and SE) and season in Fig. 3.

The monthly frequency of stagnation is highest in southern Europe and in summer (Figs. 3b,c), in line with previous studies (e.g., Horton et al. 2012; Garrido-Perez et al. 2018; Maddison et al. 2021). More than two-thirds of summer days are identified as stagnant in southwest and southeast Europe, where weather conditions are consistently calm and dry. Stagnation in southern Europe is less frequent in spring and winter (Figs. 3a,d). In contrast, there is infrequent stagnation in NEU year round, particularly in winter, when fewer than five days per month are identified as stagnant. Stagnation frequencies in Scandinavia lie between those in southern Europe and NEU.

The multimodel mean bias in the GCMs monthly stagnation frequency is shown in Fig. 4 for each region, season, and method. Overall, biases in stagnation frequency are often, but not always, of the same sign in the GCM ensemble and of

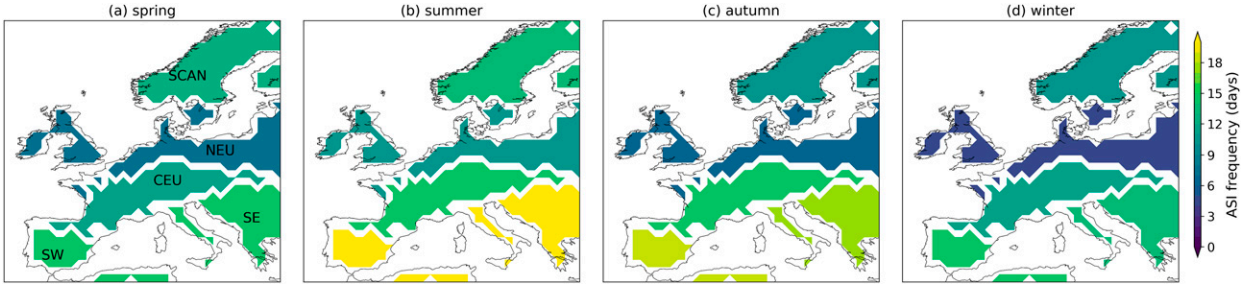

FIG. 3. Regional monthly frequency of air stagnation defined in the Horton et al. (2012) ASI in (a) spring, (b) summer, (c) autumn, and (d) winter for the historical period (1981–2010) in ERA5.

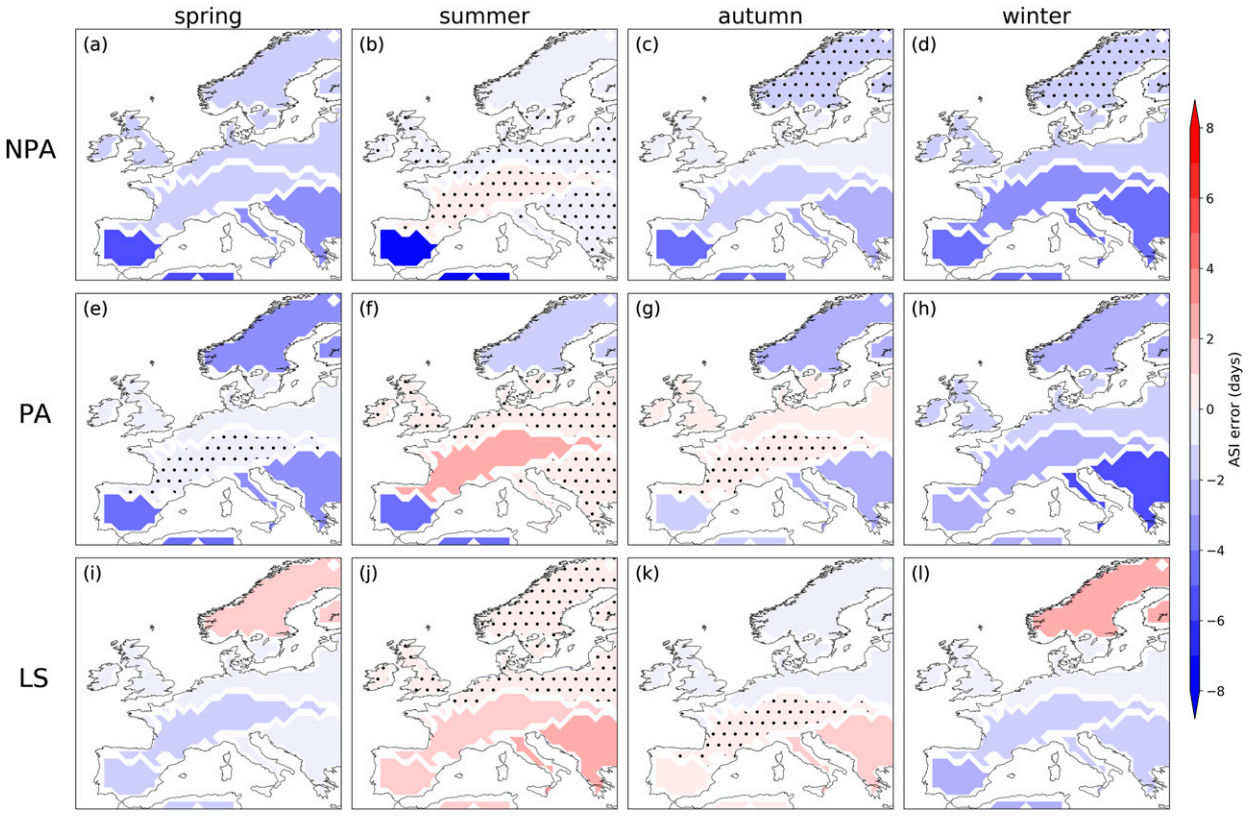

FIG. 4. Error (GCM ensemble minus ERA5) in the monthly frequency of air stagnation in the historical period (1981–2010) in the three approaches used to identify stagnation: (top) the NPA ASI, (middle) the PA ASI, and (bottom) as predicted from the larger-scale flow. The errors are shown for each region and season. Stippling shows where less than two-thirds of the models agree on the sign of the error.

comparable magnitude for the three approaches, with a generalized tendency toward an underestimation. However, there are variations in this behavior across regions, seasons, and methods. For comparison, the error in the historical frequency of stagnation in the three methods relative to the frequency in ERA5 is shown in Fig. S1. This relative error is low (generally between +15% and −15%) for most regions and seasons and all methods (and larger in the NPA than the PA ASI). It is larger during winter (where stagnation is underestimated between 20% and 40%) and over SW year round (around −30%). Model-relative errors are thus more often higher for the NPA ASI than the PA ASI, as expected. The PA method normally results in less demanding thresholds to identify stagnation in GCMs (at least for the surface wind and precipitation components) and hence increases stagnation frequency [in agreement with Garrido-Perez et al. (2022)]. This overall yields an improvement by reducing the generalized underestimation of the NPA ASI, although can result in an increased bias in some regions with overestimation, for example, CEU summer stagnation (Figs. 4b,f). Importantly, the statistical model is able to predict a similar stagnation frequency to that in ERA5 using *only* the GCMs large-scale predictors. Indeed, the maximum regional underestimation and overestimation of the LS ASI is 2.9 and 2.2 days (or −19% and 21% relative error), respectively, which is lower than in the NPA approach. Further tests have been performed with other metrics that account for compensation of errors (e.g., RMSE), yielding similar conclusions. Across all regions and seasons, the mean RMSE in the monthly frequency of stagnant days is 8.2 for NPA, 7.7 for PA, and 6.5 for the LS ASI.

On the other hand, there are seasonal variations in the magnitude and sign of biases. Stagnation in both the NPA and PA ASI is generally less frequent in the GCMs than in ERA5, particularly in spring and winter (Figs. 4a,d,e,h) and SW Europe (Figs. 4a–h). Stagnation is also less frequent than in ERA5 when predicted by the LS model during spring and winter (Figs. 4i,l), though the bias is somewhat smaller than in the other approaches, except for Scandinavia, where it predicts too much stagnation. The generalized GCM underestimation of stagnation in spring and winter is likely a result of a consistent underestimation in blocking, a major driver of European stagnation events [e.g., Maddison et al. (2021); see also section 5a]. On the contrary, summer and autumn stagnation tend to be overestimated by the LS ASI (Figs. 4j,k) and to some extent by the PA ASI (at least in half of the regions), whereas the NPA ASI continues showing too little stagnation in those seasons (except in central European summer; Fig. 4b).

Regarding the GCM performance in stagnation variability, the mean absolute biases (in days with respect to ERA5 ASI) are −0.4 for NPA, −0.02 for PA, and −1.5 for LS (Fig. S2).

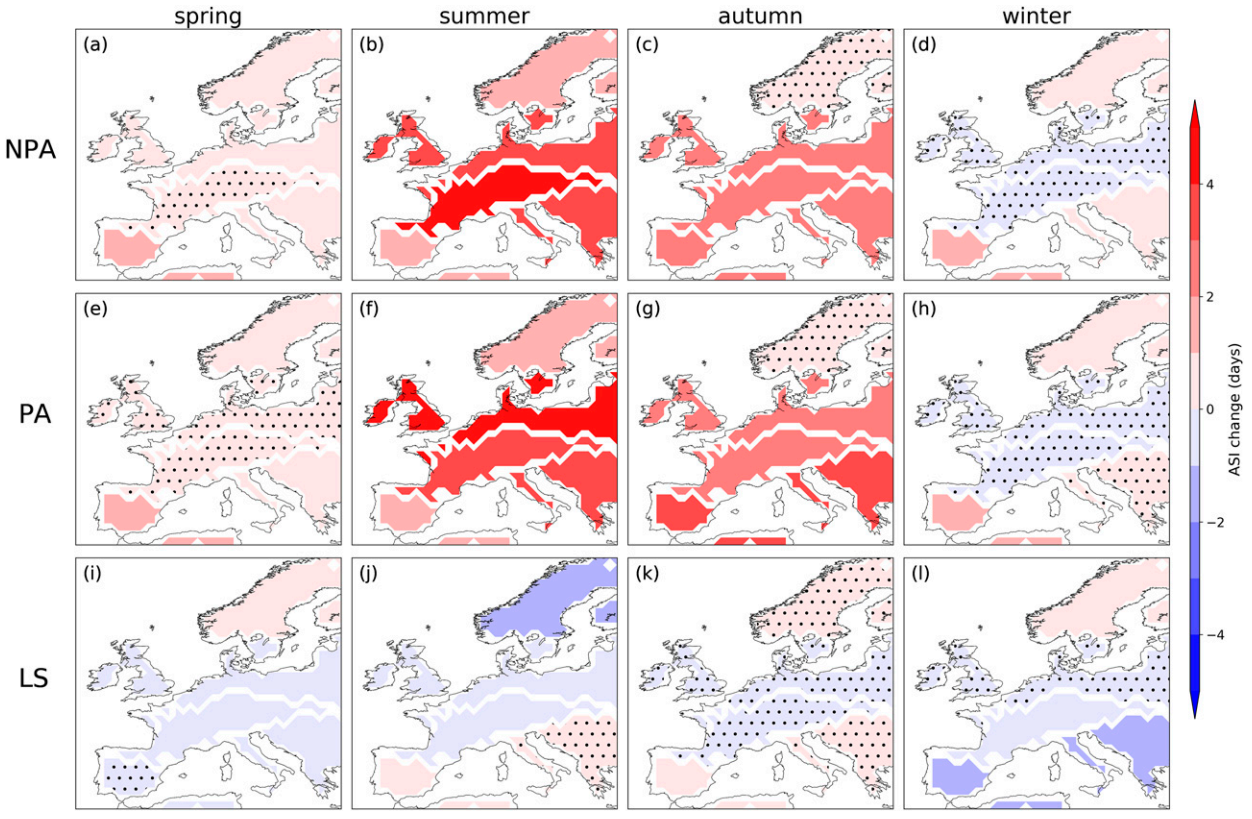

FIG. 5. Projected changes (2071–2100 minus 1981–2010) in the regional monthly frequency of air stagnation in the three approaches used to identify stagnation: (top) the NPA ASI, (middle) the PA ASI, and (bottom) as predicted from the larger-scale flow. Stippling shows where less than two-thirds of the models agree on the sign of the change.

Correcting the low percentiles of the ASI components brings an improved representation of variability in the PA approach, whereas the statistical model has the largest error in variability, partially because stagnation is predicted from the less variable large scale, which does not account for all of the ASI variance. Additional analyses confirm that the reduced variability of the LS ASI is due to the large-scale predictors and not a result of using the ERA5 relationships for the models. Therefore, the statistical model alleviates much of the stagnation deficit in GCMs but at the same time reduces its monthly variability.

5. Projected changes in stagnation frequency

The projected changes in monthly air-stagnation frequency are shown in Fig. 5 for each season and the three stagnation identification methods. Considerable increases are found in summer and autumn air-stagnation frequency (Figs. 5b,c,f,g), in agreement with previous studies (Horton et al. 2012, 2014). This is true for the NPA and PA ASIs, which means that the distributions of wind speed and precipitation shift in a way that is favorable for air stagnation, regardless of the exact threshold values used in the ASI definition. Positive trends are also found for the ASIs in southern Europe and Scandinavia in spring and winter, although the trends are small. In contrast, projected changes in the LS ASI show little change or decrease in the predicted stagnation frequency (Figs. 5i–l). These features are generally consistent among the GCMs (shown by the lack of stippling in Fig. 5), that is, the increases in stagnation frequency projected by the NPA and PA ASIs in summer and autumn are found in the majority of GCMs, as are the decreases in spring and winter LS ASI. The absence of changes in summer and autumn LS ASI is a robust feature and not the result of opposite responses across the multimodel ensemble (Fig. S3). The summer and autumn stagnation increases in the NPA and PA ASIs, and lack thereof in the LS ASI, are also evident when considering the percentage change relative to the historical frequency, where the increases typically range from 20% to 50% (Fig. S4).

To pinpoint the causes of the projected increases in stagnation, in the following sections we address three questions. Why does the LS ASI not project an increase in stagnation frequency? Which ASI components are driving the projected changes in stagnation frequency? And how do changes in the ASI components relate to known climate change impacts?

a. Projected stagnation trends in the statistical model

In this section, we focus on the distinctive behavior of the LS ASI projections and the underlying causes. First, different tests were carried out to confirm that the LS ASI projections

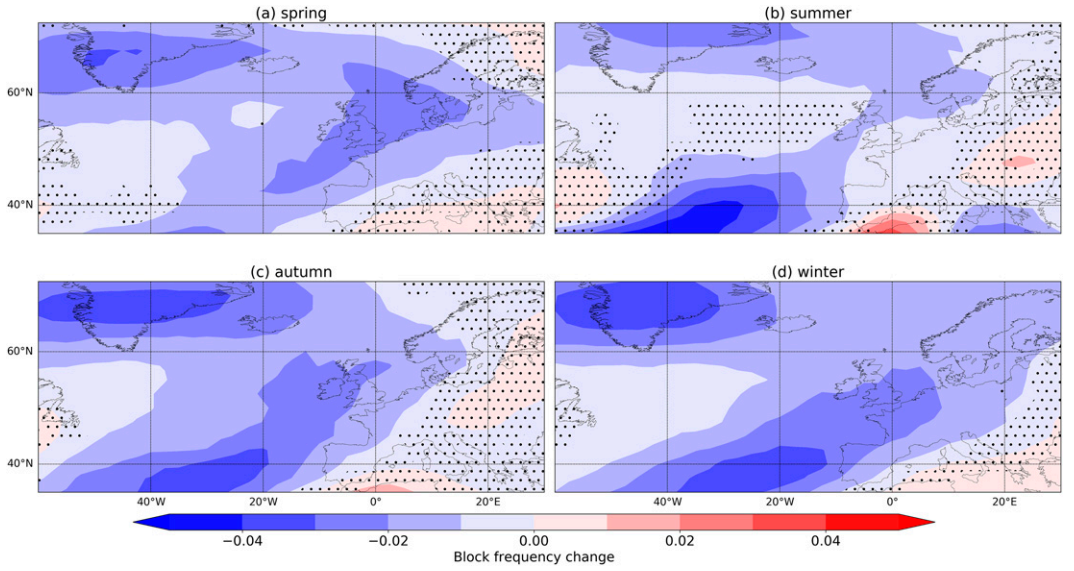

FIG. 6. Projected changes in the frequency (fraction of days blocked per season) of blocking in (a) spring, (b) summer, (c) autumn, and (d) winter. Stippling shows regions where there is less than a two-thirds agreement among the GCMs.

are not an artifact of the statistical model used. We obtained similar results to those of Figs. 5i–l when the statistical models were entirely constructed from the GCM output (Fig. S5), meaning that imposing the ERA5 relationships to the GCM predictors is not biasing the LS ASI projections. We also note that the skill of the statistical models constructed from the GCM output is similar to that in ERA5, implying that GCMs capture reasonably well the relationship between stagnation and the predictors. Second, we tested whether the linkages between ASI and the large-scale predictors retrieved from the historical period still hold in the future (i.e., that the statistical model can be applied in climate change scenarios). The results indicated that the model skill, predictors, and regression coefficients are similar for statistical models trained on the historical and future periods. Across all GCMs, regions, and seasons, more than two-thirds of predictors included in the statistical models of the historical period are also included in the models trained in the future. Together, these results reveal no substantial changes in the relationship between the large-scale circulation and stagnation. Consequently, the overall weak changes in the LS ASI are not due to a reduced influence of the large-scale circulation in stagnation in the future. Instead, other variables that are not present in the LS ASI but that influence stagnation must be playing a role.

Therefore, we finally investigated the synoptic- to large-scale circulation changes that are promoting a decrease in spring and winter stagnation frequency (and no increase in summer and autumn). We focused on blocking as the main potential driver of the LS ASI projections, since this is the most important weather system in the statistical model of regional air stagnation (Maddison et al. 2021, their Fig. 10). Several reasons further support disregarding the other predictors. First, subtropical ridges and the subtropical jet do not show substantial changes in the future (not shown), and hence they cannot explain the projected changes in LS ASI. Second, the seasons with the largest changes in LS ASI are not strongly influenced by the eddy-driven jet, which, in addition, shows no robust future changes, with some GCMs projecting increases in jet speed and others a decrease or small change (e.g., Lee et al. 2021). Figure 6 shows the multimodel-mean projected future change in the seasonal blocking frequency, that is, the change in the fraction of days in a season with blocking occurrence.

GCMs project a decrease in the frequency of blocking across the North Atlantic–European region in every season, in accordance with previous studies (e.g., Davini and D'Andrea 2020). This is particularly robust (shown by the lack of stippling) for northwestern Europe and Greenland and extends over continental Europe during spring and winter, exactly when the statistical model predicts decreases in stagnation frequency. A reduction in continental block frequency would not be expected to be concurrent with an increase in stagnation frequency (as suggested by the ASIs; Figs. 5a,d,e,h). Indeed, the regional changes in stagnation frequency predicted by the LS approach correlate well ($R^2 \approx 0.4$–0.6) with the changes in the frequency of the regional blocking predictors among the GCMs, especially for northern regions and for all seasons apart from summer. Therefore, the projected decreases in winter and spring LS ASI are substantially influenced by concurrent decreases in continental blocking (cf. Figs. 6a,d and 5i,l). There is less agreement among the GCMs in the projected changes in block frequency in summer and autumn, particularly to the east (Figs. 6b,c), in agreement with previous studies (e.g., Woollings et al. 2018). For these seasons, blocking is projected to increase over some regions (e.g., SE in summer and autumn). However, these blocking trends are small and not robust, in agreement with the absence of substantial changes in LS ASI during summer and autumn (cf. Figs. 6b,c and 5j,k). If any, they would involve much smaller increases in summer and

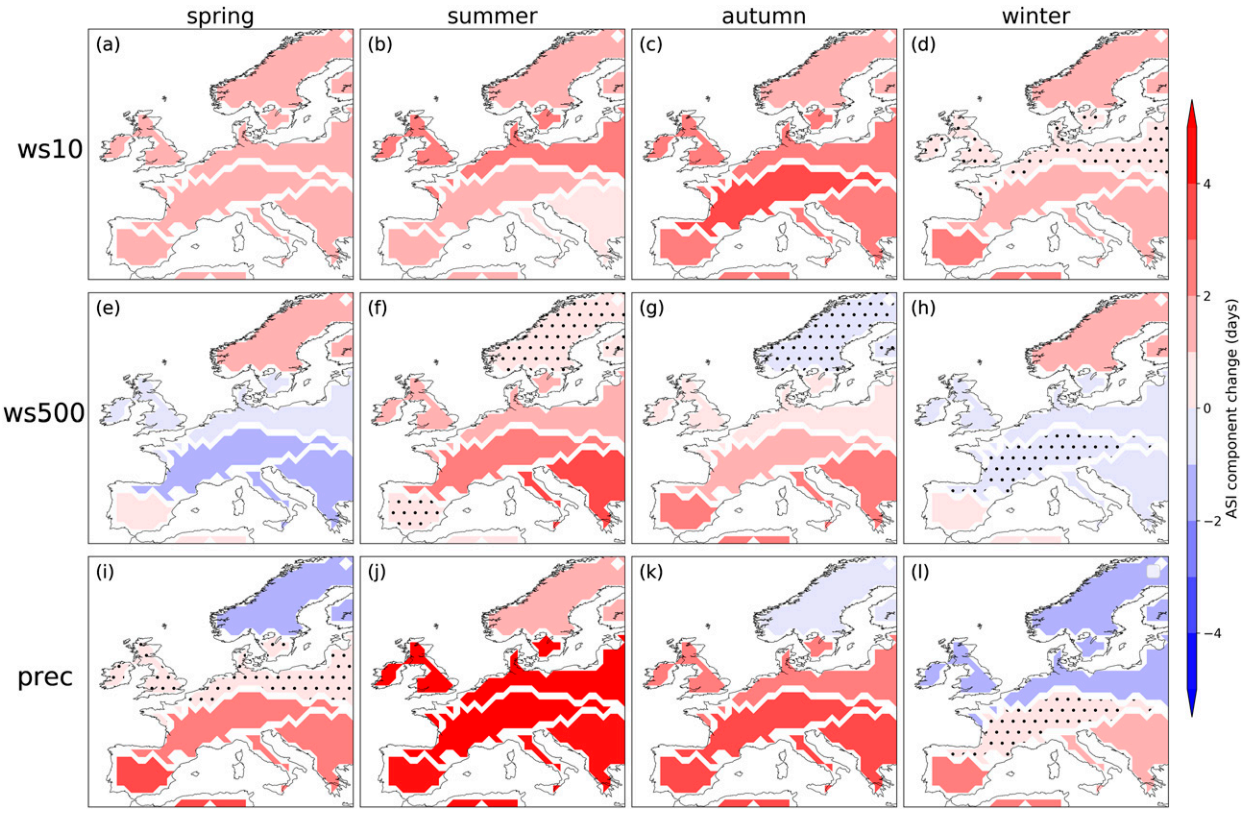

FIG. 7. Projected changes in the monthly frequency of days in which the ASI component criteria are met: (top) wind speed at 10 m, (middle) wind speed at 500 hPa, and (bottom) precipitation. Changes are shown for the NPA ASI. Stippling shows where less than two-thirds of the models agree on the sign of the change.

autumn stagnation than projected by the ASIs (Figs. 5b,c,f,g). Hence, the projected increases in the ASIs do not appear to be driven by blocking in summer and autumn.

This analysis demonstrates that future changes in dynamical features of the atmospheric circulation (i.e., an atmosphere with less frequent blocking and/or a more intense jet) cannot explain the projected increases in stagnation frequency found using the other ASI indices. Hence, the changes seen in future stagnation are largely coming from ASI drivers not related to the large-scale flow. To further explore the causes behind the projected trends in stagnation, future changes in the individual ASI components are assessed in the next subsection.

b. *Projected stagnation trends in the ASI components*

Figure 7 shows the projected changes in the monthly frequency of air stagnation when the three components of the ASI (surface wind speed, wind speed at 500 hPa, and precipitation) are considered separately. For brevity, here only the NPA ASI is shown.

The increases in air stagnation are generally apparent in all ASI components and the majority of GCMs (Fig. 7), particularly during summer and autumn, explaining the largest stagnation increases of these seasons. This is not the case in spring, when the frequency of low-wind-speed days in the midtroposphere decreases (Fig. 7e), in line with the reduction in block frequency in this season (Fig. 6a). This counteracts the increases in stagnation induced by changes in the frequency of dry days and low-surface-wind-speed days (Figs. 7a,i), resulting in the small trends projected in the spring NPA ASI (Fig. 5a). For the seasons with the largest stagnation changes (summer and autumn), the strongest increase is typically seen in the precipitation component, suggesting that dry days will become more frequent in this climate change scenario and that this drying trend is the dominant factor of the projected increases in stagnation. The precipitation component was also shown to drive future stagnation increases for most of Europe in Garrido-Perez et al. (2022), in agreement with the results shown here.

More frequent dry days in the future have been identified in GCMs in previous studies (e.g., Polade et al. 2014; Caserini et al. 2017), particularly for areas around the Mediterranean. It may seem counterintuitive that the projected increase in dry days is not accompanied by concurrent changes in the large-scale atmospheric patterns associated with stagnation (e.g., more frequent European blocking). However, precipitation may be less connected to the larger-scale circulation, particularly in summer, explaining why the statistical model did not predict a corresponding increase in future stagnation. We can test this hypothesis by assessing the relationship between the large-scale drivers and precipitation (frequency of dry days). To do this, we used the same large-scale predictors

of stagnation employed in section 2b to construct statistical models that predict the monthly frequency of dry days (rather than the stagnation frequency). These models yield similar skills for the historical and future periods (with R^2 values generally between 0.4 and 0.6, as in the LS ASI model), suggesting the precipitation is related to the same extent to the large-scale flow in the future. Like for stagnation, future changes in the frequency of dry days predicted by the large-scale circulation are small (not shown). Therefore, changes in the large-scale predictors do not explain the increases in dry days projected by the multimodel ensemble. We conclude that the projected increases in ASI are to a large extent driven by concurrent increases in the frequency of dry days, which is in turn disconnected from the large-scale flow. Assuming that the large-scale circulation aspects that are relevant for stagnation are reasonably captured by the considered drivers, and that their relationships with stagnation can be considered stationary, this result suggests that the robust multimodel trends in stagnation are not driven by changes in major large-scale dynamical factors. Possible factors not considered herein and deserving further research include thermodynamical processes linked to global/regional warming, as well as regional and local phenomena not captured by the large-scale predictors.

6. Discussion and conclusions

Increases in summer and autumn stagnation, as those reported herein, could have important implications for air quality. According to the most recent European Environment Agency report (European Environment Agency 2020), particulate matter (PM) frequently exceeded the EU limits for much of southeastern and eastern Europe (in data from 2018). For ozone, exceedances above the EU threshold were also frequent for stations located in all of the regions considered here (minus SCAN), with the highest concentrations across central and southern Europe. Future increases in stagnation will exacerbate these problems if emissions are not reduced and may result in other regions frequently exceeding the daily limit of PM, as well as more frequent days with extreme ozone concentrations, particularly in summer when the ozone and stagnation correspondence is strongest (Garrido-Perez et al. 2019).

Here, we assess the representation of air stagnation over Europe in current GCMs and its future changes using three approaches. Two rely on the direct identification of stagnation with an ASI, using either pre-established (NPA) or GCM-adapted (PA) thresholds for the underlying variables. The third one is a statistical model based on the synoptic- to large-scale atmospheric circulation (LS ASI). The latter was motivated by the apparent biases in the GCM variables used in air-stagnation indices. The statistical model only requires variables describing regional aspects of the large-scale atmospheric circulation, which tend to have smaller biases than those required for the ASIs. The assessment is performed seasonally, at the European level, and for different regions with homogeneous behavior in stagnation.

PA and NPA ASIs capture the spatial patterns of stagnation but can have substantial biases in the monthly frequency of air stagnation when compared with ERA5. Although the PA ASI displayed reduced errors in the majority of cases, regional biases still persist, showing a generalized underestimation (of up to 40% in winter). For many regions and seasons, the statistical model performed better than (or at least not worse than) ASIs and thus can be used as an alternative when dynamically driven aspects of air stagnation are pursued.

The projected changes in air stagnation under the SSP5–8.5 high-emission scenario are generally robust across the multimodel ensemble but reveal discrepancies among the three methods. The complete ASIs (both with and without percentile adjustment) project an increase in summer and autumn stagnation and little change in spring and winter, in agreement with the annual increases reported in previous studies (e.g., Horton et al. 2012, 2014; Caserini et al. 2017; Hong et al. 2019). Differently, the statistical model predicted little change in stagnation frequency in summer and autumn. This was the case for two different implementations of the statistical model, one constructed with the true (ERA5) relationships between the ASI and the large-scale predictors and one fully constructed with GCM output (containing GCM biases in the ASI but also the simulated links between the large-scale circulation and stagnation).

The generalized absence of stagnation increases predicted by the statistical model were largely attributed to small or nonrobust changes in the large-scale drivers, dominated by blocking. For winter and spring, projected decreases in atmospheric blocking act toward regional decreases in stagnation, opposite to the projected increases in ASI. Overall, changes in other dynamical drivers considered here (e.g., the eddy-driven and subtropical jets) did not appear conducive to future stagnation increases, either. As the relationships between stagnation and the circulation aspects considered here largely remain unchanged in the future, we conclude that the projected increases in the ASI are not driven by changes in its major dynamical drivers.

Future increases in summer and autumn stagnation are accompanied by corresponding increases in the three components of the ASI (i.e., the frequency of dry days, weak surface winds, and low wind speeds in the troposphere) with the strongest increases corresponding to the precipitation component. This suggests that these stagnation changes are promoted primarily by more frequent dry days, in agreement with the recent study of Garrido-Perez et al. (2022), where precipitation was identified as a key driver of future stagnation over most of Europe.

The projected tendency to drying is not incompatible with the small changes in the large-scale drivers of stagnation. To delve further into this issue, Fig. 8 summarizes the projected changes in precipitation for the GCMs used in this article. The change in annual mean precipitation is similar to previous studies (Giorgi and Lionello 2008; Ulbrich et al. 2013; IPCC 2013), with robust decreases in southern Europe and increases in regions farther north (Fig. 8a). Pfahl et al. (2017) demonstrated that this heterogeneity in European precipitation trend is driven primarily by the dynamics (while the thermodynamical response was nearly uniform globally), which is also the case in other regions of the globe (Ali and Mishra 2018; Sudharsan et al. 2020;

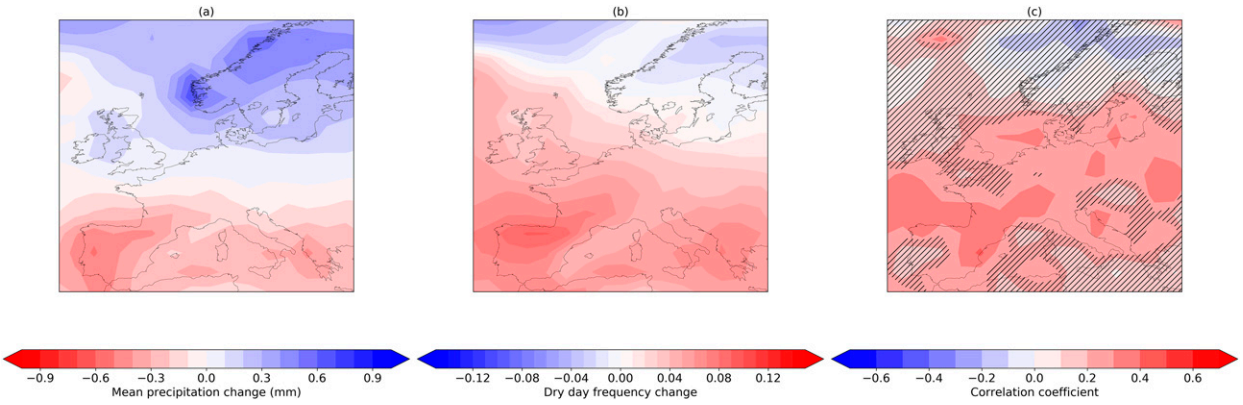

FIG. 8. (a) Projected changes (2071–2100 minus 1981–2010) in the daily accumulated precipitation, (b) projected changes in the frequency of dry days, and (c) the correlation among the GCMs between their annual global-mean temperature change and their dry-day frequency change during summer and autumn (nonsignificant correlations at the 90% confidence level denoted with hashing).

Chang et al. 2022). However, these studies consider mean precipitation rates and/or high extreme values, which may not be representative for the left tail of the precipitation distribution (i.e., that including dry days). When the analysis focuses on the frequency of low-precipitation days (defined as those with precipitation below 1 mm; Fig. 8b), a consistent increase appears over the continent (except for Scandinavia), including regions where mean precipitation experiences small changes or even increases (cf. Figs. 8a and 8b). Therefore, the projected increases in stagnation are to a large extent determined by robust increases in the frequency of dry days, neither of which can be explained by concurrent changes in the large-scale dynamics. The ultimate causes of these changes deserve further investigation. Potential factors include thermodynamical processes as well as regional/local phenomena not captured by the large-scale predictors. As the projected increases in stagnation are generally consistent across the model ensemble, local processes are likely to be less critical for these changes as they would be expected to vary among the GCMs because of their different parameterizations and resolutions. Hence, we hypothesize that robust thermodynamical aspects of climate change are likely driving the projected increases in drying and thus in stagnation frequency. This is supported by the spatially homogeneous pattern of projected increases in the frequency of dry days (Fig. 8b) as compared to that in mean precipitation (Fig. 8a). Moreover, the projected increases in dry-day frequency during summer and autumn (when stagnation changes are largest) are positively correlated with the annual global warming in the multimodel ensemble across much of the European continent (Fig. 8c). An increase in the frequency of dry days has been found in previous studies (e.g., Polade et al. 2014). For most of Europe (except Scandinavia), consecutive dry days are also projected to increase (particularly in southern Europe) under a high-emission future climate scenario similar to the one considered here (e.g., Sillmann et al. 2013).

A thermodynamically driven increase in dry-day frequency would not be captured in the model based on large-scale dynamics and can be reconciled with the absence of increased future stagnation in the statistical model. This lack of future increase is also not expected to be sensitive to the choice of ASI. Maddison et al. (2021) showed that the large-scale circulation was related similarly to stagnation as defined in three different ASIs, with similar explained variances, predictors, and regression coefficients. Therefore, future changes in stagnation related to the large-scale circulation tend to oppose those arising from nondynamical influences, regardless of the ASI used. Further work is required to elucidate if and how much of the projected stagnation trends are controlled by thermodynamics and what influence regional–local-scale circulation changes have. In this sense, regional climate models provide an alternative approach for studying air stagnation, as they will better resolve local processes and may potentially reduce the GCM biases for the variables used in the ASI. These models also project increases in air-stagnation frequency (as well as in pollutant levels if emissions of precursors are fixed at current levels) over different regions of the globe (Trail et al. 2013; Menut et al. 2013; Hong et al. 2019; Kim et al. 2020), supporting the results found here and in other studies using ASIs. Further work is required to identify the drivers of stagnation trends in regional climate model simulations.

Acknowledgments. This work has been funded by the Spanish Ministerio de Economía, Industria y Competitividad, under Grant CGL2017-83198-R (STEADY), and the Ministerio de Ciencia Innovación y Universidades, under Grant RTI2018-096402-B-I00 (JeDiS). IRS was supported by the National Center for Atmospheric Research, which is a major facility sponsored by the National Science Foundation under the Cooperative Agreement 1852977, and JMGP was supported by a Predoctoral Research Grant awarded by the Spanish Ministerio de Educación, Cultura y Deporte (FPU16/01972).

Data availability statement. The CMIP6 data are publicly available through the Earth System Grid Federation (https://esgf-node.llnl.gov/projects/cmip6/). ERA5 data are available from the Copernicus Climate Change Service Climate Data Store (https://cds.climate.copernicus.eu/#!/search?text=ERA5&type=dataset).

REFERENCES

Ali, H., and V. Mishra, 2018: Contributions of dynamic and thermodynamic scaling in subdaily precipitation extremes in India. *Geophys. Res. Lett.*, **45**, 2352–2361, https://doi.org/10.1002/2018GL077065.

Barmpadimos, I., C. Hueglin, J. Keller, S. Henne, and A. S. H. Prévôt, 2011: Influence of meteorology on PM_{10} trends and variability in Switzerland from 1991 to 2008. *Atmos. Chem. Phys.*, **11**, 1813–1835, https://doi.org/10.5194/acp-11-1813-2011.

Carro-Calvo, L., C. Ordóñez, R. García-Herrera, and J. L. Schnell, 2017: Spatial clustering and meteorological drivers of summer ozone in Europe. *Atmos. Environ.*, **167**, 496–510, https://doi.org/10.1016/j.atmosenv.2017.08.050.

Caserini, S., P. Giani, C. Cacciamani, S. Ozgen, and G. Lonati, 2017: Influence of climate change on the frequency of daytime temperature inversions and stagnation events in the Po Valley: Historical trend and future projections. *Atmos. Res.*, **184**, 15–23, https://doi.org/10.1016/j.atmosres.2016.09.018.

Catto, J. L., C. Jakob, and N. Nicholls, 2013: A global evaluation of fronts and precipitation in the ACCESS model. *Aust. Meteor. Oceanogr. J.*, **63**, 191–203, https://doi.org/10.22499/2.6301.012.

Chang, M., B. Liu, B. Wang, C. Martinez-Villalobos, G. Ren, and T. Zhou, 2022: Understanding future increases in precipitation extremes in global land monsoon regions. *J. Climate*, **35**, 1839–1851, https://doi.org/10.1175/JCLI-D-21-0409.1.

Christensen, J. H., F. Boberg, O. B. Christensen, and P. Lucas-Picher, 2008: On the need for bias correction of regional climate change projections of temperature and precipitation. *Geophys. Res. Lett.*, **35**, L20709, https://doi.org/10.1029/2008GL035694.

Davini, P., and F. D'Andrea, 2020: From CMIP3 to CMIP6: Northern Hemisphere atmospheric blocking simulation in present and future climate. *J. Climate*, **33**, 10021–10038, https://doi.org/10.1175/JCLI-D-19-0862.1.

Dawson, J. P., B. J. Bloomer, D. A. Winner, and C. P. Weaver, 2014: Understanding the meteorological drivers of U.S. particulate matter concentrations in a changing climate. *Bull. Amer. Meteor. Soc.*, **95**, 521–532, https://doi.org/10.1175/BAMS-D-12-00181.1.

European Environment Agency, 2020: Air quality in Europe—2020 report. EEA Rep. 9/2020, 160 pp., https://www.eea.europa.eu//publications/air-quality-in-europe-2020-report.

Eyring, V., S. Bony, G. A. Meehl, C. A. Senior, B. Stevens, R. J. Stouffer, and K. E. Taylor, 2016: Overview of the Coupled Model Intercomparison Project Phase 6 (CMIP6) experimental design and organization. *Geosci. Model Dev.*, **9**, 1937–1958, https://doi.org/10.5194/gmd-9-1937-2016.

Flato, G., and Coauthors, 2013: Evaluation of climate models. *Climate Change 2013: The Physical Science Basis*, T. F. Stocker et al., Eds., Cambridge University Press, 741–866, https://doi.org/10.1017/CBO9781107415324.020.

Gao, Y., and Coauthors, 2020: The climate impact on atmospheric stagnation and capability of stagnation indices in elucidating the haze events over North China Plain and northeast China. *Chemosphere*, **258**, 127335, https://doi.org/10.1016/j.chemosphere.2020.127335.

Garrido-Perez, J. M., C. Ordóñez, and R. García-Herrera, 2017: Strong signatures of high-latitude blocks and subtropical ridges in winter PM_{10} over Europe. *Atmos. Environ.*, **167**, 49–60, https://doi.org/10.1016/j.atmosenv.2017.08.004.

——, ——, ——, and D. Barriopedro, 2018: Air stagnation in Europe: Spatiotemporal variability and impact on air quality. *Sci. Total Environ.*, **645**, 1238–1252, https://doi.org/10.1016/j.scitotenv.2018.07.238.

——, ——, ——, and J. L. Schnell, 2019: The differing impact of air stagnation on summer ozone across Europe. *Atmos. Environ.*, **219**, 117062, https://doi.org/10.1016/j.atmosenv.2019.117062.

——, R. García-Herrera, and C. Ordóñez, 2021: Assessing the value of air stagnation indices to reproduce PM10 variability in Europe. *Atmos. Res.*, **248**, 105258, https://doi.org/10.1016/j.atmosres.2020.105258.

——, C. Ordóñez, D. Barriopedro, R. García-Herrera, J. L. Schnell, and D. E. Horton, 2022: A storyline view of the projected role of remote drivers on summer air stagnation in Europe and the United States. *Environ. Res. Lett.*, **17**, 014026, https://doi.org/10.1088/1748-9326/ac4290.

Giorgi, F., and P. Lionello, 2008: Climate change projections for the Mediterranean region. *Global Planet. Change*, **63**, 90–104, https://doi.org/10.1016/j.gloplacha.2007.09.005.

Hamburger, T., and Coauthors, 2011: Overview of the synoptic and pollution situation over Europe during the EUCAARI-LONGREX field campaign. *Atmos. Chem. Phys.*, **11**, 1065–1082, https://doi.org/10.5194/acp-11-1065-2011.

Hersbach, H., and Coauthors, 2020: The ERA5 global reanalysis. *Quart. J. Roy. Meteor. Soc.*, **146**, 1999–2049, https://doi.org/10.1002/qj.3803.

Hong, C., and Coauthors, 2019: Impacts of climate change on future air quality and human health in China. *Proc. Natl. Acad. Sci. USA*, **116**, 17193–17200, https://doi.org/10.1073/pnas.1812881116.

Horton, D. E., Harshvardhan, and N. S. Diffenbaugh, 2012: Response of air stagnation frequency to anthropogenically enhanced radiative forcing. *Environ. Res. Lett.*, **7**, 044034, https://doi.org/10.1088/1748-9326/7/4/044034.

——, C. B. Skinner, D. Singh, and N. S. Diffenbaugh, 2014: Occurrence and persistence of future atmospheric stagnation events. *Nat. Climate Change*, **4**, 698–703, https://doi.org/10.1038/nclimate2272.

Huang, Q., X. Cai, J. Wang, Y. Song, and T. Zhu, 2018: Climatological study of the boundary-layer air stagnation index for China and its relationship with air pollution. *Atmos. Chem. Phys.*, **18**, 7573–7593, https://doi.org/10.5194/acp-18-7573-2018.

IPCC, 2013: *Climate Change 2013: The Physical Science Basis*. Cambridge University Press, 1535 pp., https://doi.org/10.1017/CBO9781107415324.

Jacob, D. J., and D. A. Winner, 2009: Effect of climate change on air quality. *Atmos. Environ.*, **43**, 51–63, https://doi.org/10.1016/j.atmosenv.2008.09.051.

Kerr, G. H., and D. W. Waugh, 2018: Connections between summer air pollution and stagnation. *Environ. Res. Lett.*, **13**, 084001, https://doi.org/10.1088/1748-9326/aad2e2.

Kim, D.-H., J.-U. Kim, T.-J. Kim, J.-Y. Byon, J.-W. Kim, S.-H. Kwon, and Y.-H. Kim, 2020: Characteristics of air stagnation over the Korean Peninsula and projection using regional climate model of HadGEM3-RA. *Atmosphere*, **30**, 377–390, https://doi.org/10.14191/ATMOS.2020.30.4.377.

Kumar, S., V. Merwade, J. L. Kinter III, and D. Niyogi, 2013: Evaluation of temperature and precipitation trends and long-term persistence in CMIP5 twentieth-century climate simulations. *J. Climate*, **26**, 4168–4185, https://doi.org/10.1175/JCLI-D-12-00259.1.

Lee, D., S.-Y. S. Wang, L. Zhao, H. C. Kim, K. Kim, and J.-H. Yoon, 2020: Long-term increase in atmospheric stagnant conditions over northeast Asia and the role of greenhouse gases-driven warming. *Atmos. Environ.*, **241**, 117772, https://doi.org/10.1016/j.atmosenv.2020.117772.

Lee, J.-Y., and Coauthors, 2021: Future global climate: Scenario-based projections and near-term information. *Climate Change 2021: The Physical Science Basis*, V. Masson-Delmotte et al., Eds., Cambridge University Press, 553–672, https://www.ipcc.ch/report/ar6/wg1/downloads/report/IPCC_AR6_WGI_Chapter04.pdf.

Leibensperger, E. M., L. J. Mickley, and D. J. Jacob, 2008: Sensitivity of US air quality to mid-latitude cyclone frequency and implications of 1980–2006 climate change. *Atmos. Chem. Phys.*, **8**, 7075–7086, https://doi.org/10.5194/acp-8-7075-2008.

Leung, D. M., A. P. K. Tai, L. J. Mickley, J. M. Moch, A. van Donkelaar, L. Shen, and R. V. Martin, 2018: Synoptic meteorological modes of variability for fine particulate matter ($PM_{2.5}$) air quality in major metropolitan regions of China. *Atmos. Chem. Phys.*, **18**, 6733–6748, https://doi.org/10.5194/acp-18-6733-2018.

Maddison, J. W., M. Abalos, D. Barriopedro, R. García-Herrera, J. M. Garrido-Perez, and C. Ordóñez, 2021: Linking air stagnation in Europe with the synoptic- to large-scale atmospheric circulation. *Wea. Climate Dyn.*, **2**, 675–694, https://doi.org/10.5194/wcd-2-675-2021.

Meehl, G. A., and Coauthors, 2007: Global climate projections. *Climate Change 2007: The Physical Science Basis*, S. Solomon et al., Eds., Cambridge University Press, 747–846.

Mehran, A., A. AghaKouchak, and T. J. Phillips, 2014: Evaluation of CMIP5 continental precipitation simulations relative to satellite-based gauge-adjusted observations. *J. Geophys. Res. Atmos.*, **119**, 1695–1707, https://doi.org/10.1002/2013JD021152.

Menut, L., O. P. Tripathi, A. Colette, R. Vautard, E. Flaounas, and B. Bessagnet, 2013: Evaluation of regional climate simulations for air quality modelling purposes. *Climate Dyn.*, **40**, 2515–2533, https://doi.org/10.1007/s00382-012-1345-9.

O'Neill, B. C., and Coauthors, 2016: The Scenario Model Intercomparison Project (ScenarioMIP) for CMIP6. *Geosci. Model Dev.*, **9**, 3461–3482, https://doi.org/10.5194/gmd-9-3461-2016.

Ordóñez, C., D. Barriopedro, R. García-Herrera, P. M. Sousa, and J. L. Schnell, 2017: Regional responses of surface ozone in Europe to the location of high-latitude blocks and subtropical ridges. *Atmos. Chem. Phys.*, **17**, 3111–3131, https://doi.org/10.5194/acp-17-3111-2017.

——, ——, and ——, 2019: Role of the position of the North Atlantic jet in the variability and odds of extreme PM_{10} in Europe. *Atmos. Environ.*, **210**, 35–46, https://doi.org/10.1016/j.atmosenv.2019.04.045.

Oswald, E. M., L.-A. Dupigny-Giroux, E. M. Leibensperger, R. Poirot, and J. Merrell, 2015: Climate controls on air quality in the northeastern U.S.: An examination of summertime ozone statistics during 1993–2012. *Atmos. Environ.*, **112**, 278–288, https://doi.org/10.1016/j.atmosenv.2015.04.019.

Pfahl, S., P. A. O'Gorman, and E. M. Fischer, 2017: Understanding the regional pattern of projected future changes in extreme precipitation. *Nat. Climate Change*, **7**, 423–427, https://doi.org/10.1038/nclimate3287.

Polade, S. D., D. W. Pierce, D. R. Cayan, A. Gershunov, and M. D. Dettinger, 2014: The key role of dry days in changing regional climate and precipitation regimes. *Sci. Rep.*, **4**, 4364, https://doi.org/10.1038/srep04364.

Riahi, K., and Coauthors, 2017: The shared socioeconomic pathways and their energy, land use, and greenhouse gas emissions implications: An overview. *Global Environ. Change*, **42**, 153–168, https://doi.org/10.1016/j.gloenvcha.2016.05.009.

Scherrer, S. C., M. Croci-Maspoli, C. Schwierz, and C. Appenzeller, 2006: Two-dimensional indices of atmospheric blocking and their statistical relationship with winter climate patterns in the Euro-Atlantic region. *Int. J. Climatol.*, **26**, 233–249, https://doi.org/10.1002/joc.1250.

Shen, L., L. J. Mickley, and A. P. K. Tai, 2015: Influence of synoptic patterns on surface ozone variability over the eastern United States from 1980 to 2012. *Atmos. Chem. Phys.*, **15**, 10 925–10 938, https://doi.org/10.5194/acp-15-10925-2015.

Sillmann, J., V. V. Kharin, X. Zhang, F. W. Zwiers, and D. Bronaugh, 2013: Climate extremes indices in the CMIP5 multimodel ensemble: Part 1. Model evaluation in the present climate. *J. Geophys. Res. Atmos.*, **118**, 1716–1733, https://doi.org/10.1002/jgrd.50203.

Sousa, P. M., R. M. Trigo, D. Barriopedro, P. M. M. Soares, and J. A. Santos, 2018: European temperature responses to blocking and ridge regional patterns. *Climate Dyn.*, **50**, 457–477, https://doi.org/10.1007/s00382-017-3620-2.

Sudharsan, N., S. Karmakar, H. J. Fowler, and V. Hari, 2020: Large-scale dynamics have greater role than thermodynamics in driving precipitation extremes over India. *Climate Dyn.*, **55**, 2603–2614, https://doi.org/10.1007/s00382-020-05410-3.

Tai, A. P. K., L. J. Mickley, and D. J. Jacob, 2010: Correlations between fine particulate matter ($PM_{2.5}$) and meteorological variables in the United States: Implications for the sensitivity of $PM_{2.5}$ to climate change. *Atmos. Environ.*, **44**, 3976–3984, https://doi.org/10.1016/j.atmosenv.2010.06.060.

——, ——, ——, E. M. Leibensperger, L. Zhang, J. A. Fisher, and H. O. T. Pye, 2012: Meteorological modes of variability for fine particulate matter ($PM_{2.5}$) air quality in the United States: Implications for $PM_{2.5}$ sensitivity to climate change. *Atmos. Chem. Phys.*, **12**, 3131–3145, https://doi.org/10.5194/acp-12-3131-2012.

Trail, M., A. P. Tsimpidi, P. Liu, K. Tsigaridis, Y. Hu, A. Nenes, and A. G. Russell, 2013: Downscaling a global climate model to simulate climate change over the US and the implication on regional and urban air quality. *Geosci. Model Dev.*, **6**, 1429–1445, https://doi.org/10.5194/gmd-6-1429-2013.

Ulbrich, U., and Coauthors, 2013: Past and current climate changes in the Mediterranean region. *Air, Sea and Precipitation and Water*, A. Navarra and L. Tubiana, Eds., Vol. 1, *Regional Assessment of Climate Change in the Mediterranean*, Springer, 9–51.

Vautard, R., A. Colette, E. Van Meijgaard, F. Meleux, G. J. van Oldenborgh, F. Otto, I. Tobin, and P. Yiou, 2018: Attribution of wintertime anticyclonic stagnation contributing to air pollution in western Europe. *Bull. Amer. Meteor. Soc.*, **99** (Suppl.), S70–S75, https://doi.org/10.1175/BAMS-D-17-0113.1.

Wang, J. X. L., and J. K. Angell, 1999: Air stagnation climatology for the United States (1948–1998). NOAA/Air Resource Laboratory ATLAS 1, 10 pp., https://www.nrc.gov/docs/ML0722/ML072260075.pdf.

Wang, X., R. E. Dickinson, L. Su, C. Zhou, and K. Wang, 2018: $PM_{2.5}$ pollution in China and how it has been exacerbated by terrain and meteorological conditions. *Bull. Amer. Meteor. Soc.*, **99**, 105–119, https://doi.org/10.1175/BAMS-D-16-0301.1.

Webber, C. P., H. F. Dacre, W. J. Collins, and G. Masato, 2017: The dynamical impact of Rossby wave breaking upon UK PM_{10} concentration. *Atmos. Chem. Phys.*, **17**, 867–881, https://doi.org/10.5194/acp-17-867-2017.

WHO, 2021: *WHO Global Air Quality Guidelines: Particulate Matter ($PM_{2.5}$ and PM_{10}), Ozone, Nitrogen Dioxide, Sulfur Dioxide and Carbon Monoxide*. World Health Organization, 273 pp.

Woollings, T., A. Hannachi, and B. Hoskins, 2010: Variability of the North Atlantic eddy-driven jet stream. *Quart. J. Roy. Meteor. Soc.*, **136**, 856–868, https://doi.org/10.1002/qj.625.

——, and Coauthors, 2018: Blocking and its response to climate change. *Curr. Climate Change Rep.*, **4**, 287–300, https://doi.org/10.1007/s40641-018-0108-z.